

Intrinsic nonlinear valley Nernst effect in the strained bilayer graphene

Ying-Li Wu¹, Jia-Liang Wan¹, and Xiao-Qin Yu^{1*}

¹ School of Physics and Electronics, Hunan University, Changsha 410082, China

We theoretically analyze the nonlinear valley Nernst effect (NVNE) as the second-order response of temperature gradient through the semiclassical framework of electron dynamics up to second order. Our study shows that an intrinsic nonlinear pure valley current can be generated vertically to the applied temperature in the materials with both inversion and time-reversal symmetries. This intrinsic NVNE has a quantum origin from the quantum metric and shows independence from the relaxation time. It's found that the local largest symmetry near the valleys for the nonvanishing intrinsic NVNE is a single mirror symmetry in two-dimensional systems. We theoretically investigate the intrinsic NVNE in the uniaxially strained gapless bilayer graphene and find the intrinsic NVNE can emerge when applying the temperature gradient vertically to the direction of strain. Interestingly, a transition from the compressive strain to the tensile one results in the sign reversal of the intrinsic NVNE.

I. INTRODUCTION

The generation of valley current is a vital issue in valleytronics^{1–5} in which information is stored and carried through the valley (an extra degree of freedom of electron), rather than electron, in the two-dimensional (2D) crystal with a honeycomb lattice structure. A conventional method to generate valley current is via the valley Hall effect (VHE)^{4–6}, which describes carriers in two inequivalent valleys (K and K') moving towards opposite edges perpendicular to an applied electric field due to the nonzero Berry curvature (BC) of the energy band. VHE exhibits a linear dependence on the electric field.

Recently, a subfield research field to valleytronics has emerged, valley caloritronics^{7–9}, which explores thermal methods to generate valley current rather than through the electrical approach. Both valley Seebeck effect (VSE)^{9,10} and valley Nernst effect (VNE)^{11,12} have been proposed to thermally generate the valley current. Unlike VSE (a longitudinal effect), VNE refers to a transverse phenomenon, in which a linear temperature-gradient-dependent valley current is generated vertically to an applied temperature gradient. Yu *et al.*¹¹ have shown that VNE is also attributed to the BC of the occupied energy band like VHE. However, one might notice that both VHE and VNE originating from the BC as a first-order response to driving forces (electric field or temperature gradient) disappear in the nonmagnetic centrosymmetric materials since the BC becomes zero throughout the whole Brillouin zone when systems are both time-reversal (\mathcal{T}) and inversion (\mathcal{P}) symmetric. Obviously, the suppression of these linear effects (VHE and VNE) in nonmagnetic centrosymmetric materials greatly limits the selection range of valley materials.

The discovery of the nonlinear anomalous Hall effect (NAHE)^{13–15} as a second-harmonic response to an ac electric field by Sodemann in 2015, which is attributed to BC dipole instead of BC, has attracted broad interests in the exploration of the higher-order transport phenomena stemming from the other quantum geometric quantities beyond BC. A series of novel nonlinear transport phenomena are identified, including nonrecip-

rocal magnetoresistance (NMTR)¹⁶, intrinsic planar Hall effect (IPHE)^{17,18}, nonlinear Nernst effect^{19–23}, and nonlinear thermal Hall effect^{24–28}. It's found that the quantum metric^{16,18,29–32}, a quantum geometric quantity describing the relative distance between quantum states, can play a significant role in NAHE, NMTR and IPHE.

Unlike the BC, the quantum metric can exist in the systems with both \mathcal{P} - and \mathcal{T} -symmetries³³. Rooting in the quantum metric, Kamal Das *et al.*³⁴ have recently proposed a new type of valley effect, namely nonlinear valley Hall effect (NVHE), to generate valley current flowing vertically to the electric field in tilted Dirac materials containing both \mathcal{T} and \mathcal{P} symmetries. They show that NVHE emerges from an electric-field correction to the BC as a second-order response to the electric field and is independent of the relaxation time τ . Subsequently, NVHE has also been predicted in a bilayer transition metal dichalcogenide with \mathcal{P} symmetry³⁵. These two works show that a pure valley current can also be generated perpendicularly to the applied electric field in the nonmagnetic centrosymmetric materials, which tremendously broadens the range of valley materials.

In this paper, we theoretically explore the thermally driven nonlinear valley Nernst effect (NVNE) [Fig. 1] as a second-order response to the temperature gradient through the semiclassical theory in the nonmagnetic centrosymmetric materials, in which both \mathcal{P} and \mathcal{T} symmetries are present. Additionally, we also systematically analyze both global and local symmetry constraints on NVNE. Our study shows that the intrinsic NVNE (independent of τ) originating from the quantum metric can exist in materials with both global \mathcal{T} and \mathcal{P} symmetries, and the largest local symmetry near the valleys in 2D systems for a nonvanishing intrinsic NVNE is a single mirror symmetry. The formulas of the nonlinear thermoelectric coefficients (NTCs) originating from the intrinsic, BC, and Drude contributions are determined, and the symmetry constraints on the thermally driven linear and nonlinear valley (charge) currents are analyzed and discussed in Sec. II. A correction stemming from the temperature gradient to the orbital magnetic moment (OMM) is introduced and discussed in Sec. III. The effec-

tive Hamiltonian of the strained gapless trigonal-warped bilayer graphene is given, and its symmetry is analyzed in Sec. IV. The behaviours of the intrinsic NVNE for the strained bilayer graphene are discussed in Sec. V. Finally, a conclusion is given in Sec. VI.

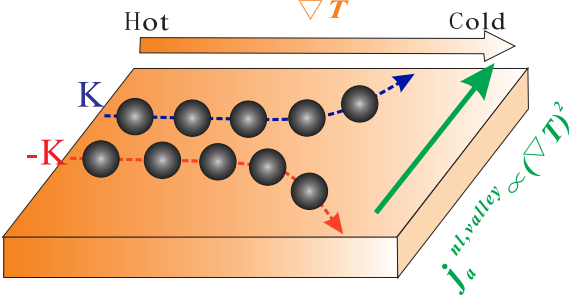


FIG. 1. Schematic of the nonlinear valley Nernst effect. A transverse nonlinear valley Nernst current $\propto (\nabla T)^2$ is generated as a second-order response to the longitudinal temperature gradient in \mathcal{P} - and \mathcal{T} -symmetric materials, where the linear valley current and transverse linear (nonlinear) charge Nernst current disappear.

II. THEORETICAL DERIVATION AND ANALYSIS

It has been established that the linear anomalous valley Nernst current $j_a^{\text{valley}} \equiv \alpha_{ab}^{\text{valley}} \partial_b T$, where $j_a^{\text{valley}} = j_a^K - j_a^{K'}$ and $\alpha_{ab}^{\text{valley}} = \alpha_{ab}^K - \alpha_{ab}^{K'}$ with the distinct valleys specified by K and K' , can't exist in \mathcal{P} -symmetric systems with \mathcal{T} symmetry. That's because the linear anomalous valley Nernst coefficient $\alpha_{ab}^{\text{valley}}$ is restricted to be even under \mathcal{T} symmetry but odd under \mathcal{P} symmetry since the valley current j_a^{valley} keeps unchanged under \mathcal{T} or \mathcal{P} operation ($j_a^K \xrightarrow{\mathcal{T} \text{ or } \mathcal{P}} -j_a^{K'}$, $j_a^{K'} \xrightarrow{\mathcal{T} \text{ or } \mathcal{P}} -j_a^K$) while the temperature gradient $\partial_b T$ remains unchanged under \mathcal{T} but changes sign under \mathcal{P} . As a result, $\alpha_{ab}^{\text{valley}}$ is forced to be zero in presence of both \mathcal{P} and \mathcal{T} symmetries, meaning $j_a^{\text{valley}} = 0$. In this background, our sight turns into the nonlinear response and investigate the nonlinear valley Nernst current $j_a^{\text{nl, valley}}$ (where the superscript "nl" represents nonlinear) whose concept roots in the nonlinear charge thermoelectric response specified by $j_a^{\text{nl}} = \alpha_{abc} \partial_b T \partial_c T$. $j_a^{\text{nl, valley}}$ is defined as $j_a^{\text{nl, valley}} = \alpha_{abc}^{\text{valley}} \partial_b T \partial_c T$ with

$$\alpha_{abc}^{\text{valley}} = \alpha_{abc}^K - \alpha_{abc}^{K'}. \quad (1)$$

Based on the dependence on the scale of the relaxation time τ , we decompose the nonlinear thermoelectric currents j_a^{nl} in a direction into three components as $j_a^{\text{nl}} = j_{1,a}^{\text{nl}}(\tau^0) + j_{2,a}^{\text{nl}}(\tau^1) + j_{3,a}^{\text{nl}}(\tau^2)$ with $j_{i(=1,2,3),a}^{\text{nl}} = \alpha_{abc,i} \partial_b T \partial_c T$. The NTCs $\alpha_{abc,1} \propto \tau^0$, $\alpha_{abc,2} \propto \tau$ and $\alpha_{abc,3} \propto \tau^2$ are disclosed to originate from the quantum metric, BC, and Drude contribution, respectively

(see the details in Appendix A). Therefore, we rewrite the coefficients $[\alpha_{abc,1}, \alpha_{abc,2}, \alpha_{abc,3}]$ as $[\alpha_{abc}^{\text{in}}, \alpha_{abc}^{\text{B}}, \alpha_{abc}^{\text{D}}]$, where superscript "in", "B", and "D" represents intrinsic, Berry, and Drude, respectively. After a tedious derivation in Appendix A, the NTCs $[\alpha_{abc}^{\text{in}}, \alpha_{abc}^{\text{B}}, \alpha_{abc}^{\text{D}}]$ are determined as, respectively,

$$\alpha_{abc}^{\text{in}} = \frac{e}{\hbar} \sum_n \int [d\mathbf{k}] \frac{(\varepsilon_{\mathbf{k}}^n - E_f)^2}{T^2} \frac{\partial f_0}{\partial \varepsilon_{\mathbf{k}}^n} \chi_{abc}^n(\mathbf{k}), \quad (2)$$

$$\alpha_{abc}^{\text{B}} = -\frac{e\tau}{\hbar} \epsilon_{abd} \sum_n \int [d\mathbf{k}] \frac{(\varepsilon_{\mathbf{k}}^n - E_f)^2}{T^2} v_c^n \frac{\partial f_0}{\partial \varepsilon_{\mathbf{k}}^n} \Omega_d^n(\mathbf{k}) \quad (3)$$

$$\alpha_{abc}^{\text{D}} = \frac{e\tau^2}{T^2} \sum_n \int [d\mathbf{k}] \frac{(\varepsilon_{\mathbf{k}}^n - E_f)^2}{m_{ab}(\mathbf{k})} v_c^n \frac{\partial f_0}{\partial \varepsilon_{\mathbf{k}}^n}, \quad (4)$$

where $\int [d\mathbf{k}]$ is shorthand for $\int d\mathbf{k}/(2\pi)^d$ with d denoting the dimension of the system, f_0 is the equilibrium Fermi-Dirac distribution function, ϵ_{abd} presents the Levi-Civita symbol, $\mathbf{v}^n(\mathbf{k}) = \langle u_n(\mathbf{k}) | \hat{\mathbf{v}} | u_n(\mathbf{k}) \rangle$ indicates the intra-band velocity matrix element for n th band determining by the periodic part of the Bloch wave-function $|u_n(\mathbf{k})\rangle$, $\varepsilon_{\mathbf{k}}^n$ denotes the n th-energy band for the unperturbed Hamiltonian, $\mathcal{A}^{nm}(\mathbf{k}) = \langle u_n(\mathbf{k}) | i\nabla_{\mathbf{k}} | u_m(\mathbf{k}) \rangle$ denotes the interband Berry connection, $\Omega_a^n(\mathbf{k}) = \sum_{m \neq n} \epsilon_{abc} \Omega_{bc}^{nm}/2$ gives the BC for the n -th band with $\Omega_{ab}^{nm}(\mathbf{k}) = i(\mathcal{A}_a^{nm} \mathcal{A}_b^{mn} - \mathcal{A}_b^{nm} \mathcal{A}_a^{mn})$ representing the band-resolved BC³⁶, $m_{ab}^{-1}(\mathbf{k}) = (1/\hbar)(\partial v_a^n / \partial k_b)$ shows the inverse effective mass tensor, and the coefficient $\chi_{abc}^n(\mathbf{k})$ is defined as

$$\chi_{abc}^n(\mathbf{k}) = \sum_{m \neq n} \hbar \left[\frac{2v_a^n \mathcal{G}_{bc}^{mn} - v_b^n \mathcal{G}_{ac}^{mn} - v_c^n \mathcal{G}_{ab}^{mn}}{(\varepsilon_{\mathbf{k}}^n - \varepsilon_{\mathbf{k}}^m)} \right], \quad (5)$$

with $\mathcal{G}_{ab}^{mn}(\mathbf{k}) = \text{Re}[\mathcal{A}_a^{nm} \mathcal{A}_b^{mn}]$ indicating the band-resolved quantum metric²⁹⁻³². The presence of the factor $\partial f_0 / \partial \varepsilon_{\mathbf{k}}^n$ in Eqs. (2)-(4) hints that the thermal-driven nonlinear current is a Fermi surface feature.

Under \mathcal{T} symmetry, the current $j_{i,a}^{\text{nl}}$ and τ change sign but $\partial_b T \partial_c T$ keeps unchanged, restricting the τ -independent part of α_{abc}^{B} \mathcal{T} -even ($\alpha_{abc}^{\text{B}}/\tau \xrightarrow{\mathcal{T}} \alpha_{abc}^{\text{B}}/\tau$) while the τ -independent part of α_{abc}^{in} and α_{abc}^{D} \mathcal{T} -odd ($\alpha_{abc}^{\text{in}} \xrightarrow{\mathcal{T}} -\alpha_{abc}^{\text{in}}$ and $\alpha_{abc}^{\text{D}}/\tau^2 \xrightarrow{\mathcal{T}} -\alpha_{abc}^{\text{D}}/\tau^2$). These \mathcal{T} -odd parities force α_{abc}^{in} and α_{abc}^{D} to vanish in the \mathcal{T} -symmetric systems. In fact, the disappearance of coefficients $[\alpha_{abc}^{\text{in}}$ and $\alpha_{abc}^{\text{D}}]$ in \mathcal{T} -symmetric systems can also be confirmed through exploiting the constraints on the quantities $[\varepsilon^n(\mathbf{k}), \mathbf{v}^n(\mathbf{k}), \Omega_{ab}^{nm}(\mathbf{k}), \mathcal{G}_{ab}^{mn}(\mathbf{k}), m_{ab}^{-1}(\mathbf{k})]$ under \mathcal{T} symmetry given in Table B1. According to those constraints, one can easily identify the integrands in Eqs. (2) and (4) are odd functions of \mathbf{k} when system is \mathcal{T} symmetric, resulting in $\alpha_{abc}^{\text{in}} = 0$ and $\alpha_{abc}^{\text{D}} = 0$. Besides, when in presence of both the \mathcal{T} and \mathcal{P} symmetries, the coefficient α_{abc}^{B} also becomes zero. That's because the BC satisfies $\Omega_{ab}^{nm}(\mathbf{k}) = -\Omega_{ab}^{nm}(-\mathbf{k})$ under \mathcal{T} symmetry and $\Omega_{ab}^{nm}(\mathbf{k}) = \Omega_{ab}^{nm}(-\mathbf{k})$ under \mathcal{P} symmetry. Subsequently, when both \mathcal{T} and \mathcal{P} symmetries are present, $\Omega_{ab}^{nm}(\mathbf{k}) = 0$ at each point in the momentum space, which leads to

TABLE I. Constraints on the in-plane tensor elements of $\alpha_{abc}^{\text{in, valley}}$ from point group symmetries. '✓' ('×') means the element is symmetry allowed (forbidden).

	global		local											
	\mathcal{P}	\mathcal{T}	\mathcal{P}	$C_{n(n>2)}^z$	$C_{n(n>2)}^x$	$C_{n(n>2)}^y$	M_z	M_x	M_y	$S_{4,6}^z$	S_4^x	S_6^x	S_4^y	S_6^y
$\alpha_{yxx}^{\text{in, valley}}$	✓	✓	×	×	×	✓	✓	✓	×	×	×	×	✓	×
$\alpha_{xyy}^{\text{in, valley}}$	✓	✓	×	×	✓	×	✓	×	✓	×	✓	×	×	×

$\alpha_{abc}^{\text{B,K}} = 0$ and $\alpha_{abc}^{\text{B,K}'} = 0$, hinting both thermal-driven nonlinear valley and charge currents stemming from the BC near the Fermi surface disappear. Therefore, the nonlinear thermal-driven current disappears in the \mathcal{P} -symmetric systems with \mathcal{T} symmetry.

Be different to the BC, the quantum metric $\mathcal{G}_{ab}^{mn}(\mathbf{k})$ can exist in presence of both \mathcal{P} and \mathcal{T} symmetries since the sign of $\mathcal{G}_{ab}^{mn}(\mathbf{k})$ keeps unchanged whether under \mathcal{T} or \mathcal{P} symmetry, namely $\mathcal{G}_{ab}^{mn}(\mathbf{k}) \xrightarrow{\mathcal{T}/\mathcal{P}} \mathcal{G}_{ab}^{mn}(-\mathbf{k})$. Hence, both the quantum metric and Drude contribution might contribute to the thermally driven nonlinear valley current in the systems with both \mathcal{T} and \mathcal{P} symmetries. In the following, we focus on the NVNE arising from the quantum metric and exclude the Drude contribution. Experimentally, the signal from the Drude contribution can be separated based on the scaling relations involving the linear conductivity $\sigma \propto \tau$: Drude contribution (quadratic to σ) and quantum metric (independent of σ^2).

In addition to the constraints from the \mathcal{T} and \mathcal{P} symmetries, the other local symmetries near the individual valleys will also impose constraints on the nonlinear coefficients $\alpha_{a'b'c'}$ for K (K') valleys as:

$$\alpha_{a'b'c'}^{\text{K/K}'} = \mathcal{R}_{a'a} \mathcal{R}_{b'b} \mathcal{R}_{c'c} \alpha_{abc}^{\text{K/K}'}, \quad (6)$$

Here, it should be point out that \mathcal{R} indicates symmetries of the low-energy $k \cdot p$ model defined for the valleys instead of the global crystalline symmetry since the local symmetries near the valleys determine the valley response instead of global crystalline symmetry³⁴. The obtained constraints on coefficients $[\alpha_{xyy}^{\text{in, valley}}, \alpha_{yxx}^{\text{in, valley}}]$ from the intrinsic contribution are summarized in Table I. According to Table I, one can easily notice that the largest local symmetry near the valleys in 2D cases for a nonvanishing $\alpha_{aa_{\perp}a_{\perp}}^{\text{in, valley}}$ is a single mirror symmetry $M_{a_{\perp}}$, where a_{\perp} indicates the coordinate axis orthogonal to axis a in the 2D plane.

III. TEMPERATURE-GRADIENT-INDUCED ORBITAL MAGNETIC MOMENT

In linear VNE, the different transverse edges will hold the oppositely OMM polarized carriers in the real space which is guaranteed by the valley contrasting OMM, i.e. $\mathbf{m}^{\text{K}}(\mathbf{k}) = -\mathbf{m}^{\text{K}'}(\mathbf{k})$. One might ask what physical quantity distinguishes the carriers separated by the intrinsic NVNE in real space since the OMM vanishes ($\mathbf{m}(\mathbf{k}) = 0$)

in the whole Brillouin zone when both \mathcal{P} and \mathcal{T} symmetries are present.

We notice that an correction to the OMM will be induced by the temperature gradient and can be nonzero when in presence of both \mathcal{P} and \mathcal{T} symmetries. The a -th component of this temperature-gradient induced OMM $m_{n,a}^{\nabla T}(\mathbf{k})$ for n band is^{37,38}

$$m_{n,a}^{\nabla T}(\mathbf{k}) = \sum_{m \neq n} \left[2\text{Re} \frac{\mathcal{M}_a^{nm} \mathcal{A}_d^{mn}}{\varepsilon_{\mathbf{k}}^n - \varepsilon_{\mathbf{k}}^m} + \frac{e}{2\hbar} \epsilon_{abc} (\partial_b \mathcal{G}_{cd}^{mn}) \right] \partial_d T, \quad (7)$$

with $\mathcal{M}^{nm} = \frac{e}{2} \sum_{l \neq m} (\mathbf{v}^{nl} + \mathbf{v}^m \delta_{nl}) \times \mathcal{A}^{lm}$ representing the interband OMM, where $\mathbf{v}^{nl}(\mathbf{k}) = \langle u_n(\mathbf{k}) | \hat{\mathbf{v}} | u_l(\mathbf{k}) \rangle$ denotes the interband velocity matrix element.

Through exploiting the constraints on the quantities $[\partial_d T, \varepsilon^n(\mathbf{k}), \mathcal{A}^{nm}(\mathbf{k}), \mathbf{v}^n(\mathbf{k}), \mathcal{G}_{ab}^{mn}(\mathbf{k})]$ under \mathcal{P}/\mathcal{T} symmetry given in Table B1, one can easily verify that the temperature-gradient induced OMM $\mathbf{m}_n^{\nabla T}(\mathbf{k})$ changes signs under both \mathcal{P} and \mathcal{T} symmetries, namely $\mathbf{m}_n^{\nabla T}(\mathbf{k}) \xrightarrow{\mathcal{T}/\mathcal{P}} -\mathbf{m}_n^{\nabla T}(-\mathbf{k})$, which hints 1) $\mathbf{m}_n^{\nabla T}(\mathbf{k})$ can exist when both \mathcal{P} and \mathcal{T} symmetries are present; 2) the nonlinear OMM satisfies $\mathbf{m}_n^{\nabla T, \text{K}}(\mathbf{k}) = -\mathbf{m}_n^{\nabla T, \text{K}'}(-\mathbf{k})$. Additionally, the entropy density $s_{n0}^{\tau_v}(\mathbf{k}) = f_0(\varepsilon_{\mathbf{k}}^n - E_f)/T + k_B T \ln[1 + \exp(-\frac{\varepsilon_{\mathbf{k}}^n - E_f}{k_B T})]$ for opposite valleys meets $s_{n0}^{\text{K}}(\mathbf{k}) = s_{n0}^{\text{K}'}(-\mathbf{k})$ in the \mathcal{T} - and \mathcal{P} -symmetric systems. As a result, the orbital magnetization $\mathbf{M}_n^{\nabla T, \tau_v} = \int_{\mathbf{K}_{\tau_v}} [d\mathbf{k}] s_{n0}^{\tau_v}(\mathbf{k}) \mathbf{m}_n^{\nabla T, \tau_v}(\mathbf{k})$ for the K valley, which stems from the temperature-gradient-induced OMM, has same magnitude but opposite signs to that for the K' valley (i.e. $\mathbf{M}_n^{\nabla T, \text{K}} = -\mathbf{M}_n^{\nabla T, \text{K}'}$), meaning that the temperature-gradient-induced orbital magnetization is valley-contrasting. Here $\int_{\mathbf{K}_{\tau_v}}$ represents the integration near τ_v valley.

Hence, when applying a temperature gradient to the materials exhibiting the two fundamental symmetries (\mathcal{T} and \mathcal{P} symmetries), the carriers in the inequivalent valleys hold opposite polarizations of orbital magnetization and flow towards opposite transverse edges in real space driven by the NVNE, hinting the intrinsic valley-contrasting orbital magnetization (VCOM) accompanies the intrinsic NVNE and distinguishes the carriers separated by the intrinsic NVNE in real space.

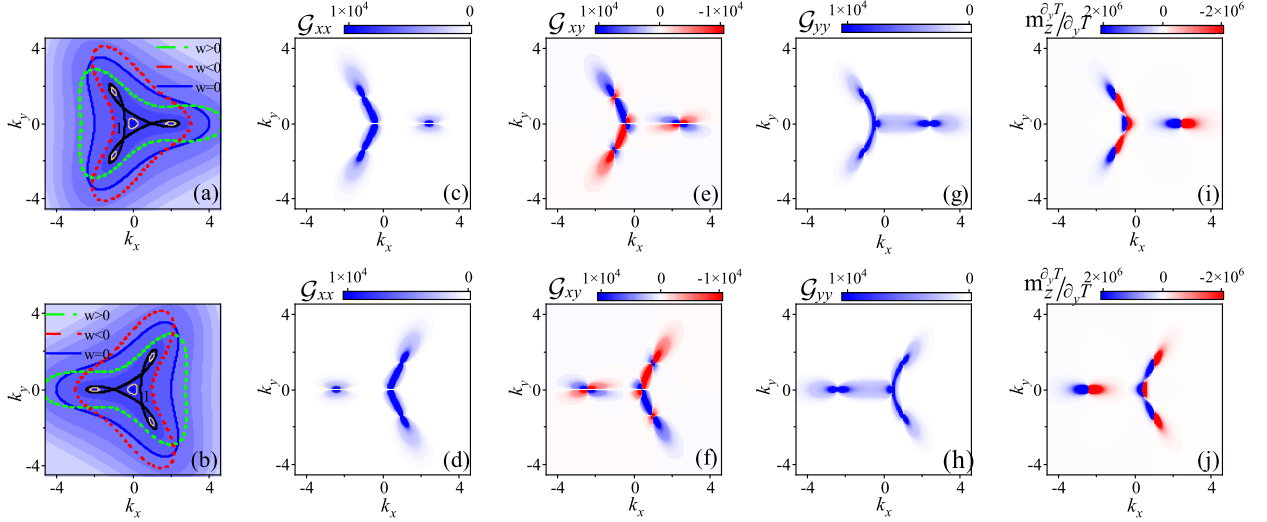


FIG. 2. Schematic of the energy contour [(a),(b)], the quantum metric elements \mathcal{G}_{xx} [(c),(d)], \mathcal{G}_{xy} [(e),(f)], \mathcal{G}_{yx} [(g),(h)] and the temperature-gradient-induced orbital magnetic moment $m_z^{\partial T}/\partial T$ [(i), (j)] of the conduction band for different valleys of trigonal warping bilayer graphene. The up (bottom) ones are for K (K') valleys, respectively. The green dash dot line (red dash line) and the solid lines in [(a),(b)] indicate energy band with the uniaxial tensile (compressive) strain and without strain, respectively. The color background in (a) and (b) represent the energy contour without strain ($w = 0$). The strength of strain $w = 1\varepsilon_L$ is fixed in (c)-(j). Momenta (energies) are measured in units of $k_L = m^*v_3/\hbar$ ($\varepsilon_L = m^*v_3^2/2$). The \mathcal{G}_{ab} and $m_z^{\partial T}/\partial T$ are measured in units of k_L^{-2} and $e/(\hbar k_L^3)$, respectively.

IV. THE EFFECTIVE HAMILTONIAN AND SYMMETRIES ANALYSIS FOR THE STRAINED BILAYER GRAPHENE

One of candidate materials to observe the intrinsic NVNE is the strained trigonal-warping bilayer graphene in the AB Bernal-stacked structure. Both global \mathcal{P} and \mathcal{T} symmetries are protected in the AB Bernal-stacked bilayer graphene since its crystal point symmetry belongs to D_{3d} ^{39–41}. Additionally, the local \mathcal{P} symmetry is lacking in the AB Bernal-stacked bilayer graphene near two valleys [Figs. 2 (a) and (b)] since its local symmetry belongs to C_{3v} (comprised of a threefold rotation C_3 and a mirror symmetry) instead of C_{6v} owing to the interlayer skew hopping. One might notice that the local C_3 symmetry near the valleys would force the intrinsic NVNE vanishing in AB Bernal-stacked bilayer graphene (Table I). However, the local C_3 symmetry can be broken through the application of a uniaxial strain, resulting in nonzero intrinsic NVNE.

In the presence of uniaxial strain along x direction, the effective low-energy Hamiltonian for τ_v ($= \pm 1, +1$ for K and -1 for K') valley of the trigonal-warping bilayer graphene^{42,43} can be expressed as

$$\hat{H}_{\tau_v} = \left(-\frac{\hbar^2(k_x^2 - k_y^2)}{2m^*} + w \right) \sigma_x - \tau_v \frac{\hbar^2 k_x k_y}{m^*} \sigma_y + \tau_v v_3 \hbar k_x \sigma_x - v_3 \hbar k_y \sigma_y, \quad (8)$$

where m^* is the effective mass directly dependent on

the interlayer coupling, w is attributed to the strain effect and depends on the strain tensors u_{xx} and u_{yy} as $w = \zeta(u_{xx} - u_{yy})$, with $\zeta = -0.443$ for the bilayer graphene⁴³, the terms in the second line originate from the interlayer skew hopping and induce a trigonal warping deformation of the Fermi circle near the Dirac cone [Figs. 2 (a) and (b)], v_3 indicates the Fermi velocity related to the interlayer skew hopping, and $\sigma_{i=x,y,z}$ represents the pauli matrix for sublattices. For simplicity, we focus on the conduction band, and the corresponding energy dispersion $\varepsilon_{\tau_v}(\mathbf{k})$, the intraband velocity matrix element $v_{\tau_v,a}(\mathbf{k})$, and the quantum metric $\mathcal{G}_{\tau_v,ab}(\mathbf{k})$ of the conduction band are found to be, respectively

$$\varepsilon_{\tau_v}(\mathbf{k}) = \sqrt{N_1^2 + N_2^2}, \quad v_{\tau_v,a}(\mathbf{k}) = \frac{N_1 N_{1a} + N_2 N_{2a}}{\sqrt{N_1^2 + N_2^2}},$$

$$\mathcal{G}_{\tau_v,ab}(\mathbf{k}) = \frac{N_2^2 N_{1a} N_{1b} + N_1^2 N_{2a} N_{2b} - N_1 N_2 (N_{1a} N_{2b} + N_{1b} N_{2a})}{4(N_1^2 + N_2^2)^2}, \quad (9)$$

where $N_1(\mathbf{k}) = -\hbar^2(k_x^2 - k_y^2)/2m^* + \tau_v v_3 \hbar k_x + w$, $N_2(\mathbf{k}) = -\tau_v \hbar^2 k_x k_y / m^* - v_3 \hbar k_y$, the variable \mathbf{k} in bracket of $N_{i(=1,2)}(\mathbf{k})$ and $N_{ij}(\mathbf{k}) = \partial[N_i(\mathbf{k})]/\partial k_{j=a,b}$ has been neglected for simplification, and the energy-band label “c” representing conduction band in the superscripts of physical quantities [ε , v and \mathcal{G}] have also been neglected for simplicity. As expected, the quantum metric elements [\mathcal{G}_{xx} , \mathcal{G}_{xy} , and \mathcal{G}_{yy}] are nonzero and satisfy $\mathcal{G}_{ab}^K(\mathbf{k}) = \mathcal{G}_{ab}^{K'}(-\mathbf{k})$ [Figs. 2(c)-(h)] in presence of \mathcal{P} and \mathcal{T} symmetries.

It should be pointed out that the effective Hamiltonian $\hat{H}_{\tau_v=+1}$ and $\hat{H}_{\tau_v=-1}$ in Eq. (8) act in the same space of two-component wave functions $\Phi = (\phi_A, \phi_{\bar{B}})$, where $\phi_{\alpha(=\bar{A},\bar{B})}$ is the electron amplitude on the sublattice α . This framework differs from the previous works^{42,43}, where the component in $\Phi_{\tau_v=-1}$ is reversed for valley K', namely $\Phi_{\tau_v=-1} = (\phi_{\bar{B}}, \phi_A)$. In this space $\Phi = (\phi_A, \phi_{\bar{B}})$, we have the time-reversal operator $\hat{T} = \sigma_0 \mathcal{K}$ with \mathcal{K} representing complex conjugation operator, inversion operator $\hat{P} = \sigma_x$, the mirror symmetries $M_x = \sigma_0$ and $M_y = \sigma_x$. Consequently, one can easily confirm that both global \mathcal{P} and \mathcal{T} symmetries are present in the strained trigonal-warping bilayer graphene since $\hat{T}\hat{H}_K(\mathbf{k})\hat{T}^{-1} = \hat{H}_{K'}(-\mathbf{k})$ and $\hat{P}\hat{H}_K(\mathbf{k})\hat{P}^{-1} = \hat{H}_{K'}(-\mathbf{k})$. On the contrary, the local \mathcal{P} , \mathcal{T} , and M_x symmetries are broken, and only the local M_y symmetry is survived owing to $\hat{T}\hat{H}_{\tau_v}(\mathbf{k})\hat{T}^{-1} \neq \hat{H}_{\tau_v}(-\mathbf{k})$, $\hat{P}\hat{H}_{\tau_v}(\mathbf{k})\hat{P}^{-1} \neq \hat{H}_{\tau_v}(-\mathbf{k})$, $\hat{M}_x\hat{H}_{\tau_v}(k_x, k_y)\hat{M}_x^{-1} \neq \hat{H}_{\tau_v}(-k_x, k_y)$ and $\hat{M}_y\hat{H}_{\tau_v}(k_x, k_y)\hat{M}_y^{-1} = \hat{H}_{\tau_v}(k_x, -k_y)$. Additionally, owing to the presence of the uniaxial strain ($w \neq 0$), the local threefold rotation C_3 is also broken since $\hat{C}_3\hat{H}_{\tau_v}(\hat{R}_{2\pi/3}\mathbf{k})\hat{C}_3^{-1} \neq \hat{H}_{\tau_v}(\mathbf{k})$ and $\hat{C}_3^2\hat{H}_{\tau_v}(\hat{R}_{-2\pi/3}\mathbf{k})(\hat{C}_3^2)^{-1} \neq \hat{H}_{\tau_v}(\mathbf{k})$, where the threefold rotation operator for the τ_v valley is expressed as $C_3 = e^{i\frac{2\pi}{3}\tau_v\sigma_z}$ and $C_3^2 = e^{-i\frac{2\pi}{3}\tau_v\sigma_z}$, and \hat{R}_θ represents the rotation operator around z -axis by $\theta(=\pm 2\pi/3)$. As a result, only the local mirror symmetry M_y is survived in the trigonal-warping bilayer graphene in presence of the uniaxial strain along x -direction.

V. RESULTS AND DISCUSSION

The global \mathcal{T} and \mathcal{P} symmetries combining with the only surviving local M_y symmetry indicate that $\alpha_{xyy}^{\text{in, valley}}$ can be nonzero but require $\alpha_{yxx}^{\text{in, valley}} = 0$ in the uniaxially strained bilayer graphene with the strain along x direction [Table I].

Therefore, we will only consider the situation in which the temperature gradient is applied along y -direction in the following. Additionally, the simultaneous existence of the global \mathcal{T} and \mathcal{P} symmetries will force the ordinary OMMs to vanish and also guarantee the values of temperature-gradient-induced OMMs $m_z^{\partial_y T}(\mathbf{k})$ has opposite sign on the inversion-symmetric side of Fermi energy for different valleys, i.e. $m_z^{\partial_y T, K}(\mathbf{k}) = -m_z^{\partial_y T, K'}(-\mathbf{k})$, in the strained trigonal-warping bilayer graphene [Figs. 2(i) and (j)]. Therefore, when applying a temperature gradient along the y -direction in strained trigonal-warping bilayer graphene, the carriers in the inequivalent valleys will not only flow toward opposite edges along x -axis due to the nonzero NVNE but also exhibit opposite polarizations of orbital magnetization (see details in Sec. III). Consequently, accompanying the NVNE, opposite polarizations of the orbital magnetization are generated along opposite edges perpendicular to the temperature gradi-

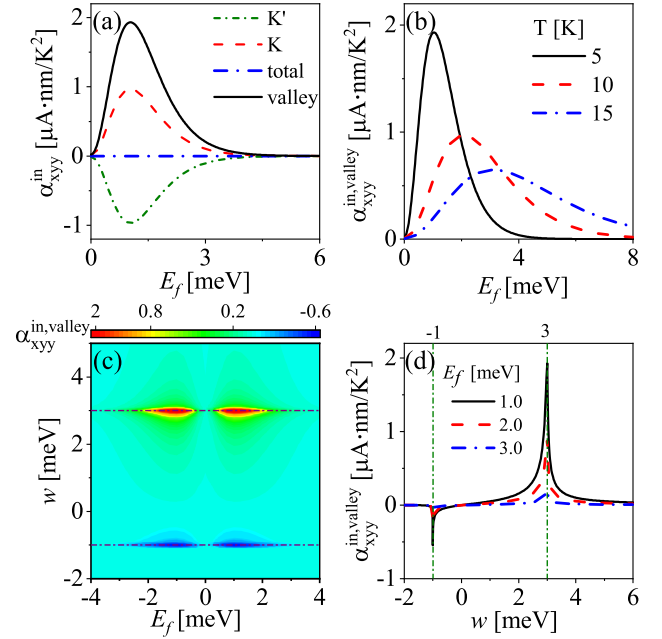


FIG. 3. (a) The quantity α_{xyy}^{nl} as a function of Fermi energy E_f for different valleys. (b) The quantity $\alpha_{xyy}^{\text{nl, valley}}$ versus the Fermi energy E_f for different temperature T . (c) The quantity $\alpha_{xyy}^{\text{nl, valley}}$ as a function of Fermi energy E_f and strain parameter w . (d) The quantity $\alpha_{xyy}^{\text{nl, valley}}$ versus w for different E_f . Momenta are measured in units of $k_L = m^*v_3/\hbar \approx 0.035 \text{ nm}^{-1}$ and the effective mass $m^* = 0.037m_e$ ⁴⁴. $T = 5 \text{ K}$ is fixed in (a) and (c). $w = 3 \text{ meV}$ is taken in (b).

ent in real space, distinguishing the carriers separated by the intrinsic NVNE in real space.

Figure 3(a) illustrates the dependence of intrinsic nonlinear Nernst coefficients α_{xyy}^{in} on the Fermi energy E_f for the different valleys in the strained trigonal-warping bilayer graphene. As expected, the α_{xyy}^{in} for the K valley has the same magnitude but opposite sign to that for the K' valley, indicating that the total intrinsic nonlinear Nernst current ($\propto \alpha_{xyy}^{\text{in, K}} + \alpha_{xyy}^{\text{in, K'}}$) vanishes but a pure intrinsic nonlinear valley Nernst current ($\propto \alpha_{xyy}^{\text{in, K}} - \alpha_{xyy}^{\text{in, K'}}$) can be generated. In addition, A peak feature of $\alpha_{xyy}^{\text{in, valley}}$ is observed near the Dirac cone which might be ascribed to the fact that the quantum metric elements achieve their maximum in this region [Figs. 2 (c)-(h)]. As the temperature T decreases, the value of the peak increases and its position shifts towards lower energy levels [Fig. 3 (b)].

The behaviour of $\alpha_{xyy}^{\text{nl, valley}}$ are significantly influenced by the strain [Figs. 3 (c) and (d)]. A transition from compressive strain ($w < 0$) to tensile strain ($w > 0$) results in the sign reversal of $\alpha_{xyy}^{\text{nl, valley}}$, which provides a potential approach for the strain type detection. Additionally, $\alpha_{xyy}^{\text{nl, valley}}$ exhibits a negative peak at $w = -1 \text{ meV}$ followed by a positive peak at $w = 3 \text{ meV}$ [Figs. 3(c) and (d)]. The appearance of these two peaks might be qualitatively attributed to the effect of strain on the rich Fermi

properties of trigonal warping bilayer graphene. For the strain-free ($w = 0$) bilayer graphene, a Lifshitz transition occurs at energy $\varepsilon_L(\mathbf{k}) = m^*v_3^2/2 \approx 1 \text{ meV}$, where the Fermi surface evolves from a single connected pocket into four distinct ones as energy and momentum decrease [Figs. 2 (a) and (b)]: the electronic dispersion consists of one central Dirac cone located at the K (K') point of the Brillouin zone and three leg Dirac cones. Previous works have demonstrated that the topology of the Fermi surface changes through the merging of Dirac cones when the strain strength is modulated^{46,47}: for $-\varepsilon_L < w \leq 3\varepsilon_L$, the electronic dispersion retains four Dirac cones in the Brillouin zone. At $w = -1 \text{ meV}$, the two Dirac cones along k_x axis merge into single point. For $w > 3 \text{ meV}$, in contrast, only the cones along the k_x axis are survived, while the other two Dirac cones disappear. Consequently, the observed two peaks precisely correspond to the strain strengths around which the number of Dirac cones decreases.

VI. CONCLUSION

We study the NVNE as a second-order response to the temperature gradient. It's found that although the linear valley effect disappears in the systems with both \mathcal{P} and \mathcal{T} symmetries, a intrinsic NVNE, stemming from the quantum metric and independent of the relaxation time, can emerge. Through analyzing the symmetry constraints on this intrinsic NVNE, we identify the largest local symmetry near the valleys in 2D systems for the nonzero intrinsic NVNE is a single local mirror symmetry. Additionally, an intrinsic valley-contrasting orbital magnetization, which originates from temperature-gradient-induced OMM, accompanies the intrinsic NVNE and can distinguish the carriers separated by the intrinsic NVNE in real space. The behaviour of the intrinsic NVNE in the uniaxially strained trigonal warping bilayer graphene has been investigated. Our study shows that the intrinsic NVNE can emerge when applying the temperature gradient vertically to the direction of strain. Interestingly, the peaks of the intrinsic NVNE versus strain parameter w precisely correspond to the strain strengths at which the number of Dirac cones decreases. In addition, when transiting the compressive strain $w < 0$ into tensile one $w > 0$, the sign of intrinsic NVNE changes.

VII. ACKNOWLEDGEMENTS

This work is supported by the National Natural Science Foundation of China (Grant No. 12004107), the National Science Foundation of Hunan, China (Grant No. 2023JJ30118), and the Fundamental Research Funds for the Central Universities.

Appendix A: The expressions of the nonlinear thermoelectric currents

In this section, the expression of nonlinear thermoelectric current density \mathbf{j}^{nl} (where the superscript “nl” represents nonlinear) as a second-order response to temperature gradient will be derived through the Boltzmann equation and semiclassical dynamical theory up to second order. Within the relaxation time approximation, the Boltzmann equation in presence of the temperature gradient ∇T and in absence of the electric field ($\mathbf{E} = 0$) and magnetic field ($\mathbf{B} = 0$) can be expressed as

$$\frac{f_{\mathbf{k}} - f_0}{\tau} = -\frac{\partial f_{\mathbf{k}}}{\partial r_a} v_a, \quad (\text{A1})$$

where $f_0 = (1 + e^{(\varepsilon_{\mathbf{k}} - E_f)/(k_B T)})^{-1}$ is the equilibrium Fermi distribution, τ represents relaxation time, v_a and r_a representing the velocity and coordinate position of electrons in the a direction, respectively. Since we are interested in the response up to the second order in the temperature gradient, we have the nonequilibrium Fermi distribution function as

$$f(\mathbf{r}, \mathbf{k}) \approx f_0(\mathbf{r}, \mathbf{k}) + \delta f_1(\partial_a T) + \delta f_2(\partial_a T \partial_b T) \quad (\text{A2})$$

with the terms δf_n understood to be vanish as $(\partial T / \partial r_a)$, where $a, b = x$ or y , and the local equilibrium Fermi distribution f_0 depends on \mathbf{r} and \mathbf{k} via indirect variables T and $\varepsilon_{\mathbf{k}}$ as $f(\mathbf{r}, \mathbf{k}) = f_0(\varepsilon_{\mathbf{k}}, T(\mathbf{r}))$. Hence, one can have

$$\frac{\partial f_0}{\partial r_a} = \frac{\partial f_0}{\partial T} \frac{\partial T}{\partial r_a} = -\frac{(\varepsilon_{\mathbf{k}} - E_f)}{T} \frac{\partial f_0}{\partial \varepsilon_{\mathbf{k}}} \partial_a T. \quad (\text{A3})$$

Accompanying Eq. (A3) with the relation $\partial \varepsilon_{\mathbf{k}} / \partial \mathbf{k} = \hbar \mathbf{v}$, we can express $\partial f_0 / \partial T$ in terms of $\partial f_0 / \partial \mathbf{k}$ as

$$\frac{\partial f_0}{\partial \mathbf{k}} = \frac{\partial f_0}{\partial \varepsilon_{\mathbf{k}}} \frac{\partial \varepsilon_{\mathbf{k}}}{\partial \mathbf{k}} = -\frac{\hbar \mathbf{v} T}{(\varepsilon_{\mathbf{k}} - E_f)} \frac{\partial f_0}{\partial T}. \quad (\text{A4})$$

Taking the expanded form of f in Eq. (A2) into Eq. (A1) and comparing the order of temperature gradient for both sides of the equation, one has

$$\begin{aligned} \delta f_1 &= -\tau \frac{\partial f_0}{\partial T} v_a \partial_a T, \\ \delta f_2 &= \tau^2 \left(\frac{\partial^2 f_0}{\partial T^2} \partial_a T \partial_b T + \frac{\partial f_0}{\partial T} \partial_{ab} T \right) v_a v_b, \end{aligned} \quad (\text{A5})$$

where we have introduce the shorthand notations $\partial_a = \partial / \partial r_a$ and $\partial_{ab} = \partial / \partial r_a \partial r_b$ for the simplification. When assuming the temperature gradient is uniform (i.e. $\partial_{ab} T = 0$), the first-order δf_1 (second-order δf_2) correction of the temperature gradient to the non-equilibrium distribution functions is found to be

$$\begin{aligned} \delta f_1 &= \frac{\tau}{T \hbar} (\varepsilon_{\mathbf{k}} - E_f) \frac{\partial f_0}{\partial k_a} \partial_a T, \\ \delta f_2 &= \tau^2 \left[2 \hbar v_b \frac{\partial f_0}{\partial k_a} + (\varepsilon_{\mathbf{k}} - E_f) \frac{\partial^2 f_0}{\partial k_a \partial k_b} \right] \\ &\quad \times \frac{\varepsilon_{\mathbf{k}} - E_f}{\hbar^2 T^2} \partial_a T \partial_b T. \end{aligned} \quad (\text{A6})$$

Besides, when further applying the temperature gradient in a single direction, one can have $a = b$.

Gao *et al.* have derived the expression of thermoelectric current density \mathbf{j} from a single Bloch band labeled by 0 through the semiclassical framework of electron dynamics up to second order.²¹ One can easily expand their formula to the multiple-band case, in which multiple-Bloch band contribution to thermoelectric current density is considered, by changing the label 0 into n (band index) and then taking a summation over n . Therefore, the total thermoelectric current density \mathbf{j} , taking the conventional term $-e \sum_n \int [d\mathbf{k}] \mathbf{v}^n f_{\mathbf{k}}$ from the carriers group velocity into consideration, is found to be

$$\begin{aligned} \mathbf{j} = & -e \sum_n \int [d\mathbf{k}] \mathbf{v}^n f_{\mathbf{k}} - \frac{\nabla T}{T} \times \frac{e}{\hbar} \sum_n \int [d\mathbf{k}] \Omega^n(\mathbf{k}) \\ & \times \left((\varepsilon_{\mathbf{k}}^n - E_f) f_{\mathbf{k}} + \frac{1}{k_B T} \ln(1 + e^{\frac{\varepsilon_{\mathbf{k}}^n - E_f}{k_B T}}) \right) \\ & + \nabla T \times \frac{e}{\hbar} \sum_n \int [d\mathbf{k}] \frac{(\varepsilon_{\mathbf{k}}^n - E_f)}{T^2} \frac{\partial f_{\mathbf{k}}}{\partial \varepsilon_{\mathbf{k}}^n} \\ & \times \left(2\hat{e}_a \hbar \sum_{m \neq n} \text{Re} \frac{\mathcal{A}_a^{nm} (\mathbf{v}^n \times \mathcal{A}^{mn})_b}{\varepsilon_{\mathbf{k}}^n - \varepsilon_{\mathbf{k}}^m} \partial_b T \right), \end{aligned} \quad (\text{A7})$$

where $\Omega^n(\mathbf{k}) = \nabla_{\mathbf{k}} \times \mathcal{A}^n(\mathbf{k})$ is the unperturbed BC, $\mathcal{A}^n(\mathbf{k}) = \langle u_n(\mathbf{k}) | i \nabla_{\mathbf{k}} | u_n(\mathbf{k}) \rangle$ denotes the intraband Berry connection with $|u_n(\mathbf{k})\rangle$ being the periodic part of the Bloch wave-function, $\mathcal{A}^{nm}(\mathbf{k}) = \langle u_n(\mathbf{k}) | i \nabla_{\mathbf{k}} | u_m(\mathbf{k}) \rangle$ representing the interband Berry connection, $\mathbf{v}^{mn}(\mathbf{k}) = \langle u_m(\mathbf{k}) | \hat{\mathbf{v}} | u_n(\mathbf{k}) \rangle$ and $\mathbf{v}^n(\mathbf{k}) = \langle u_n(\mathbf{k}) | \hat{\mathbf{v}} | u_n(\mathbf{k}) \rangle$ indicating the interband and intraband velocity matrix element, respectively. The second term is ascribed to the BC $\Omega^n(\mathbf{k})$, and the third term stems from the orbital magnetic quadrupole moment density. Obviously, both second and third terms have the quantum origins from the geometric properties of the electron wave function.

Taking the formula of the nonequilibrium distribution function $f_{\mathbf{k}}$ determined by Eqs.(A2) and (A6), the formula of the nonlinear thermoelectric current density j_a^{nl} along a direction as a second-order response to the temperature gradient in the 2D systems is determined as

$$\begin{aligned} j_a^{\text{nl}} = & \left\{ -\frac{e\tau^2}{\hbar^2} \sum_n \int [d\mathbf{k}] v_a^n \frac{(\varepsilon_{\mathbf{k}}^n - E_f)}{T^2} \left[2\hbar v_c^n \frac{\partial f_0}{\partial k_b} + (\varepsilon_{\mathbf{k}}^n - E_f) \frac{\partial^2 f_0}{\partial k_b \partial k_c} \right] - \frac{e\tau}{\hbar} \epsilon_{abd} \sum_n \int [d\mathbf{k}] \frac{(\varepsilon_{\mathbf{k}}^n - E_f)^2}{T^2} v_c^n \frac{\partial f_0}{\partial \varepsilon_{\mathbf{k}}^n} \Omega_d^n(\mathbf{k}) \right. \\ & \left. + e \sum_{m \neq n} \int [d\mathbf{k}] \frac{(\varepsilon_{\mathbf{k}}^n - E_f)^2}{T^2} \frac{\partial f_0}{\partial \varepsilon_{\mathbf{k}}^n} \left[\frac{2v_a^n \mathcal{G}_{bc}^{nm} - v_b^n \mathcal{G}_{ac}^{nm} - v_c^n \mathcal{G}_{ab}^{nm}}{\varepsilon_{\mathbf{k}}^n - \varepsilon_{\mathbf{k}}^m} \right] \right\} \partial_b T \partial_c T, \end{aligned} \quad (\text{A8})$$

where $\mathcal{G}_{ad}^{nm}(\mathbf{k}) = \text{Re}[\mathcal{A}_a^{nm} \mathcal{A}_d^{mn}]$ is the band-resolved quantum metric^{29–32}, which quantifies the distance between wave functions in the parameter space. The nonlinear thermoelectric currents j_a^{nl} in a direction can be further decomposed into three components as $j_a^{\text{nl}} = j_{1,a}^{\text{nl}}(\tau^0) + j_{2,a}^{\text{nl}}(\tau^1) + j_{3,a}^{\text{nl}}(\tau^2)$ based on the dependence on the scale of the relaxation time τ . Therefore, the corresponding nonlinear thermoelectric coefficients $\alpha_{abc,i}(=1,2,3)$, which are defined as $j_{i,a}^{\text{nl}} = \alpha_{abc,i} \partial_b T \partial_c T$,

are found to be, respectively,

$$\begin{aligned} \alpha_{abc,1} = & e \sum_{m \neq n} \int [d\mathbf{k}] \frac{(\varepsilon_{\mathbf{k}}^n - E_f)^2}{T^2} \frac{\partial f_0}{\partial \varepsilon_{\mathbf{k}}^n} \\ & \times \left[\frac{2v_a^n \mathcal{G}_{bc}^{nm} - v_b^n \mathcal{G}_{ac}^{nm} - v_c^n \mathcal{G}_{ab}^{nm}}{\varepsilon_{\mathbf{k}}^n - \varepsilon_{\mathbf{k}}^m} \right], \end{aligned} \quad (\text{A9})$$

$$\alpha_{abc,2} = -\frac{e\tau}{\hbar} \epsilon_{abd} \sum_n \int [d\mathbf{k}] \frac{(\varepsilon_{\mathbf{k}}^n - E_f)^2}{T^2} v_c^n \frac{\partial f_0}{\partial \varepsilon_{\mathbf{k}}^n} \Omega_d^n(\mathbf{k}), \quad (\text{A10})$$

$$\alpha_{abc,3} = \frac{e\tau^2}{T^2} \sum_n \int [d\mathbf{k}] \frac{(\varepsilon_{\mathbf{k}}^n - E_f)^2}{m_{ab}(\mathbf{k})} v_c^n \frac{\partial f_0}{\partial \varepsilon_{\mathbf{k}}^n} \quad (\text{A11})$$

with $m_{ab}^{-1}(\mathbf{k}) = (1/\hbar)(\partial v_a / \partial k_b)$ indicating the inverse effective mass tensor. Obviously, the nonlinear thermoelectric coefficients $\alpha_{abc,1} \propto \tau^0$, $\alpha_{abc,2} \propto \tau$ and $\alpha_{abc,3} \propto \tau^2$ are disclosed to originate from the quantum metric, BC, and Drude contributions, respectively. Hence, the coefficients $[\alpha_{abc,1}, \alpha_{abc,2}, \alpha_{abc,3}]$ have been rewritten in the

main text as $[\alpha_{abc}^{\text{in}}, \alpha_{abc}^{\text{B}}, \alpha_{abc}^{\text{D}}]$, where superscript “in”, “B”, and “D” represents intrinsic, Berry, and Drude, respectively.

Appendix B: The exploitation of the symmetry constraints

The symmetry constraints on the coefficients $[\varepsilon^n(\mathbf{k}), \mathcal{A}^{nm}(\mathbf{k}), \mathbf{v}^n(\mathbf{k}), \mathcal{G}_{ab}^{mn}(\mathbf{k})]$ from \mathcal{T} / \mathcal{P} symmetries will be exploited in the section. We firstly analyse the \mathcal{T} -symmetric constraint. In spin-less \mathcal{T} -symmetric systems, the time-reversal operator is expressed as $\mathcal{T} = \mathcal{K}$ determined by the complex conjugation operator \mathcal{K} , and the effective Hamiltonian $H(\mathbf{k})$ and the periodic part of the Bloch wave-function $|u_n(\mathbf{k})\rangle$ satisfy

$$\begin{aligned} \mathcal{T}H(\mathbf{k})\mathcal{T}^{-1} &= H(-\mathbf{k}), \\ |u_n(-\mathbf{k})\rangle &= |u_n(\mathbf{k})\rangle^*, \end{aligned} \quad (\text{B1})$$

which gives the energy eigenvalue $\varepsilon^n(\mathbf{k})$ of the effective Hamiltonian $\langle H(\mathbf{k})|u_n(\mathbf{k})\rangle = \varepsilon^n(\mathbf{k})|u_n(\mathbf{k})\rangle$ is an even function of the momentum \mathbf{k} , namely

$$\varepsilon^n(\mathbf{k}) = \varepsilon^n(-\mathbf{k}), \quad (\text{B2})$$

enforcing the group velocity $\mathbf{v}^n(\mathbf{k}) = (1/\hbar)(\partial\varepsilon^n/\partial\mathbf{k})$ odd and the inverse effective mass tensor $m_{ab}^{-1}(\mathbf{k}) = (1/\hbar)(\partial v_a^n/\partial k_b)$ even with respect to \mathbf{k} . The interband Berry connection satisfies:

$$\begin{aligned} \mathcal{A}^{mn}(-\mathbf{k}) &= \langle u_m(-\mathbf{k})|i\partial_{-\mathbf{k}}|u_n(-\mathbf{k})\rangle \\ &= -i\langle u_m(\mathbf{k})^*|\partial_{\mathbf{k}}u_n(\mathbf{k})^*\rangle \\ &= -i\langle \partial_{\mathbf{k}}u_n(\mathbf{k})|u_m(\mathbf{k})\rangle \\ &= i\langle u_n(\mathbf{k})|\partial_{\mathbf{k}}u_m(\mathbf{k})\rangle \\ &= \mathcal{A}^{nm}(\mathbf{k}). \end{aligned} \quad (\text{B3})$$

To obtaining the last second equality, we have used the relation $\langle \partial_{\mathbf{k}}u_n(\mathbf{k})|u_m(\mathbf{k})\rangle + \langle u_n(\mathbf{k})|\partial_{\mathbf{k}}u_m(\mathbf{k})\rangle = \partial_{\mathbf{k}}\langle u_n(\mathbf{k})|u_m(\mathbf{k})\rangle = 0$. Consequently, when the systems is \mathcal{T} -symmetric, BC $\Omega_{ab}^{nm}(\mathbf{k})$ and the band-resolved quantum metric $\mathcal{G}_{ab}^{nm}(\mathbf{k})$ satisfy

$$\begin{aligned} \Omega_{ab}^{nm}(\mathbf{k}) &= i[\mathcal{A}_a^{nm}(\mathbf{k})\mathcal{A}_b^{mn}(\mathbf{k}) - \mathcal{A}_b^{nm}(\mathbf{k})\mathcal{A}_a^{mn}(\mathbf{k})] \\ &= i[\mathcal{A}_a^{mn}(-\mathbf{k})\mathcal{A}_b^{nm}(-\mathbf{k}) - \mathcal{A}_b^{mn}(\mathbf{k})\mathcal{A}_a^{nm}(-\mathbf{k})] \\ &= i[\mathcal{A}_b^{nm}(-\mathbf{k})\mathcal{A}_a^{mn}(-\mathbf{k}) - \mathcal{A}_a^{nm}(-\mathbf{k})\mathcal{A}_b^{mn}(\mathbf{k})] \\ &= -\Omega_{ab}^{nm}(-\mathbf{k}) \end{aligned} \quad (\text{B4})$$

and

$$\begin{aligned} \mathcal{G}_{ab}^{nm}(\mathbf{k}) &= \frac{1}{2}\text{Re}[\mathcal{A}_a^{nm}(\mathbf{k})\mathcal{A}_b^{mn}(\mathbf{k}) + \mathcal{A}_b^{nm}(\mathbf{k})\mathcal{A}_a^{mn}(\mathbf{k})] \\ &= \frac{1}{2}\text{Re}[\mathcal{A}_a^{mn}(-\mathbf{k})\mathcal{A}_b^{nm}(-\mathbf{k}) + \mathcal{A}_b^{mn}(-\mathbf{k})\mathcal{A}_a^{nm}(-\mathbf{k})] \\ &= \frac{1}{2}\text{Re}[\mathcal{A}_b^{nm}(-\mathbf{k})\mathcal{A}_a^{mn}(-\mathbf{k}) + \mathcal{A}_a^{nm}(-\mathbf{k})\mathcal{A}_b^{mn}(-\mathbf{k})] \\ &= \mathcal{G}_{ab}^{nm}(-\mathbf{k}). \end{aligned} \quad (\text{B5})$$

Next, let's turn our sight into the symmetry constraint from \mathcal{P} symmetry. Under \mathcal{P} operation, the position vector \mathbf{r} changes sign to $-\mathbf{r}$, and the effective Hamiltonian $H(\mathbf{k})$ and the corresponding periodic part of the Bloch wave-function $|u_n(\mathbf{k})\rangle$ satisfy:

$$\begin{aligned} \mathcal{P}H(\mathbf{k})\mathcal{P}^{-1} &= H(-\mathbf{k}), \\ \mathcal{P}|u_n(\mathbf{k})\rangle &= |u_n(-\mathbf{k})\rangle, \end{aligned} \quad (\text{B6})$$

the energy eigenvalue of the Bloch Hamiltonian has following symmetry with respect to \mathbf{k}

$$\varepsilon^n(\mathbf{k}) = \varepsilon^n(-\mathbf{k}), \quad (\text{B7})$$

the symmetries of group velocity $\mathbf{v}^n(\mathbf{k})$ and the inverse effective mass tensor $m_{ab}^{-1}(\mathbf{k})$ are same to those under \mathcal{T} symmetry, namely $\mathbf{v}^n(\mathbf{k}) \xrightarrow{\mathcal{P}} -\mathbf{v}^n(-\mathbf{k})$ and $m_{ab}^{-1}(\mathbf{k}) \xrightarrow{\mathcal{P}} m_{ab}^{-1}(-\mathbf{k})$. The interband Berry connection $\mathcal{A}^{nm}(\mathbf{k})$ in the \mathcal{P} -symmetric systems meets

$$\begin{aligned} \mathcal{A}^{nm}(\mathbf{k}) &= \langle u_n(\mathbf{k})|i\partial_{\mathbf{k}}|u_m(\mathbf{k})\rangle \\ &= i\langle u_n(\mathbf{k})|\mathcal{P}^+\mathcal{P}\partial_{\mathbf{k}}|u_m(\mathbf{k})\rangle \\ &= -i\langle u_n(-\mathbf{k})|\partial_{\mathbf{k}}|u_m(-\mathbf{k})\rangle \\ &= -\mathcal{A}^{nm}(-\mathbf{k}). \end{aligned} \quad (\text{B8})$$

Therefore, Berry curvature and the quantum metric follow

$$\begin{aligned} \Omega_{ab}^{nm}(\mathbf{k}) &= i[\mathcal{A}_a^{nm}(\mathbf{k})\mathcal{A}_b^{mn}(\mathbf{k}) - \mathcal{A}_b^{nm}(\mathbf{k})\mathcal{A}_a^{mn}(\mathbf{k})] \\ &= i[\mathcal{A}_a^{nm}(-\mathbf{k})\mathcal{A}_b^{mn}(-\mathbf{k}) - \mathcal{A}_b^{nm}(-\mathbf{k})\mathcal{A}_a^{mn}(-\mathbf{k})] \\ &= \Omega_{ab}^{nm}(-\mathbf{k}) \end{aligned} \quad (\text{B9})$$

and

$$\begin{aligned} \mathcal{G}_{ab}^{nm}(\mathbf{k}) &= \frac{1}{2}\text{Re}[\mathcal{A}_a^{nm}(\mathbf{k})\mathcal{A}_b^{mn}(\mathbf{k}) + \mathcal{A}_b^{nm}(\mathbf{k})\mathcal{A}_a^{mn}(\mathbf{k})] \\ &= \frac{1}{2}\text{Re}[\mathcal{A}_a^{nm}(-\mathbf{k})\mathcal{A}_b^{mn}(-\mathbf{k}) + \mathcal{A}_b^{nm}(-\mathbf{k})\mathcal{A}_a^{mn}(-\mathbf{k})] \\ &= \mathcal{G}_{ab}^{nm}(-\mathbf{k}). \end{aligned} \quad (\text{B10})$$

According to Eqs. (B4) and (B9), one can find that $\Omega_{ab}^{nm}(\mathbf{k}) = 0$ when in presence of both \mathcal{T} and \mathcal{P} symmetries.

The a -th component of the temperature-gradient induced OMM $m_{n,a}^{\nabla T}(\mathbf{k})$ for the n -th band is written as

$$\begin{aligned} m_{n,a}^{\nabla T}(\mathbf{k}) &= \sum_{m \neq n} \left[2\text{Re} \frac{\mathcal{M}_a^{nm} \mathcal{A}_d^{mn}}{\varepsilon_{\mathbf{k}}^n - \varepsilon_{\mathbf{k}}^m} + \frac{e}{2\hbar} \epsilon_{abc} (\partial_b \mathcal{G}_{cd}^{mn}) \right] \partial_d T \\ &= \epsilon_{abc} \left[e \sum_{l \neq m} \sum_{m \neq n} \frac{\text{Re}[v_b^{nl} A_c^{lm} A_d^{mn}]}{\varepsilon_{\mathbf{k}}^n - \varepsilon_{\mathbf{k}}^m} \right. \\ &\quad \left. + e \sum_{m \neq n} \frac{\text{Re}[v_b^m A_c^{lm} A_d^{mn}]}{\varepsilon_{\mathbf{k}}^n - \varepsilon_{\mathbf{k}}^m} + \frac{e}{2\hbar} \epsilon_{abc} (\partial_b \mathcal{G}_{cd}^{mn}) \right] \partial_d T, \end{aligned} \quad (\text{B11})$$

Based on the symmetry constraints of the coefficients $[\varepsilon^n(\mathbf{k})$, $\mathbf{v}^n(\mathbf{k})$, $\mathcal{A}^{nm}(\mathbf{k})$, $\mathcal{G}_{ab}^{mn}(\mathbf{k})$ and $\partial_d T$], the temperature-gradient induced OMM $m_{n,a}^{\nabla T}(\mathbf{k})$ are, accordingly, transformed as

$$m_{n,a}^{\nabla T}(\mathbf{k}) = -m_{n,a}^{\nabla T}(-\mathbf{k}) \quad (\text{B12})$$

for both \mathcal{T} and \mathcal{P} symmetries. The above analysed transformations of the coefficients under \mathcal{P}/\mathcal{T} symmetries are summarized in Table B1.

TABLE B1. The constraints on the different quantities under time-reversal (\mathcal{T}) and inversion (\mathcal{P}) symmetries.

	\mathcal{T}	\mathcal{P}
$\partial_d T$	$-\partial_d T$	$\partial_d T$
$\varepsilon^n(\mathbf{k})$	$\varepsilon^n(-\mathbf{k})$	$\varepsilon^n(-\mathbf{k})$
$\mathbf{v}^n(\mathbf{k})$	$-\mathbf{v}^n(-\mathbf{k})$	$-\mathbf{v}^n(-\mathbf{k})$
$m_{ab}^{-1}(\mathbf{k})$	$m_{ab}^{-1}(-\mathbf{k})$	$m_{ab}^{-1}(-\mathbf{k})$
$\mathcal{A}^{nm}(\mathbf{k})$	$\mathcal{A}^{nm}(-\mathbf{k})$	$-\mathcal{A}^{nm}(-\mathbf{k})$
$\Omega_{ab}^{nm}(\mathbf{k})$	$-\Omega_{ab}^{nm}(-\mathbf{k})$	$\Omega_{ab}^{nm}(-\mathbf{k})$
$\mathcal{G}_{ab}^{nm}(\mathbf{k})$	$\mathcal{G}_{ab}^{nm}(-\mathbf{k})$	$\mathcal{G}_{ab}^{nm}(-\mathbf{k})$
$\mathbf{m}_n^{\nabla T}(\mathbf{k})$	$-\mathbf{m}_n^{\nabla T}(-\mathbf{k})$	$-\mathbf{m}_n^{\nabla T}(-\mathbf{k})$

- * yuxiaoqin@hnu.edu.cn
- ¹ D. Xiao, W. Yao, and Q. Niu, Valley-contrasting physics in graphene: Magnetic moment and topological transport, *Phys. Rev. Lett.* **99**, 236809 (2007).
 - ² A. R. Akhmerov, J. H. Bardarson, A. Rycerz, and C. W. J. Beenakker, Theory of the valley-valve effect in graphene nanoribbons, *Phys. Rev. B* **77**, 205416 (2008).
 - ³ J. R. Schaibley, H. Yu, G. Clark, P. Rivera, J. S. Ross, K. L. Seyler, W. Yao, and X. Xu, Valleytronics in 2D materials, *Nat. Rev. Mater.* **1**, 16055 (2016).
 - ⁴ W.-Y. Tong, S.-J. Gong, X.-G. Wan and C.-G. Duan, Concepts of ferrovalley material and anomalous valley Hall effect, *Nat. Commun.* **7**, 13612 (2016).
 - ⁵ R. Peng, Y.-D. Ma, X.-L. Xu, Z.-L. He, B.-B. Huang, and Y. Dai, Intrinsic anomalous valley Hall effect in single-layer Nb₃I₈, *Phys. Rev. B* **102**, 035412 (2020).
 - ⁶ D. Xiao, G.-B. Liu, W. Feng, X. Xu, and W. Yao, Coupled spin and valley physics in monolayers of MoS₂ and other group-VI dichalcogenides, *Phys. Rev. Lett.* **108**, 196802 (2012).
 - ⁷ X.-B. Chen, L. Zhang, and H. Guo, Valley caloritronics and its realization by graphene nanoribbons, *Phys. Rev. B* **92**, 155427 (2015).
 - ⁸ P. Kapri, B. Dey, and T. K. Ghosh, Valley caloritronics in a photodriven heterojunction of Dirac materials, *Phys. Rev. B* **102**, 045417 (2020).
 - ⁹ X.-C. Zhai, W.-W. Gao, X.-L. Cai, D. Fan, Z.-H. Yang, and L. Meng, Spin-valley caloritronics in silicene near room temperature, *Phys. Rev. B* **94**, 245405 (2016).
 - ¹⁰ Z. Yu, F. Xu, and J. Wang, Valley Seebeck effect in gate tunable zigzag graphene nanoribbons, *Carbon* **99**, 451 (2016).
 - ¹¹ X.-Q. Yu, Z.-G. Zhu, G. Su, and A.-P. Jauho, Thermally driven pure spin and valley currents via the anomalous Nernst effect in monolayer group-VI dichalcogenides, *Phys. Rev. Lett.* **115**, 246601 (2015).
 - ¹² M. T. Dau, C. Vergnaud, A. Marty, C. Beigné, S. Gambarelli, V. Maurel, T. Journot, B. Hyot, T. S. Guillet, B. Grévin, H. Okuno, and M. Jamet, The valley Nernst effect in WSe₂, *Nat. Commun.* **10**, 5796 (2019).
 - ¹³ I. Sodemann and L. Fu, Quantum nonlinear Hall effect induced by Berry curvature dipole in time-reversal invariant materials, *Phys. Rev. Lett.* **115**, 216806 (2015).
 - ¹⁴ T. Low, Y. Jiang, and F. Guinea, Topological currents in black phosphorus with broken inversion symmetry, *Phys. Rev. B* **92**, 235447 (2015).
 - ¹⁵ Z. Z. Du, C. M. Wang, H.-Z. Lu, and X. C. Xie, Band Signatures for Strong Nonlinear Hall Effect in Bilayer WTe₂, *Phys. Rev. Lett.* **121**, 266601 (2018).
 - ¹⁶ D. Kaplan, T. Holder, and B. Yan, Unification of Nonlinear Anomalous Hall Effect and Nonreciprocal Magnetoresistance in Metals by the Quantum Geometry, *Phys. Rev. Lett.* **132**, 026301 (2024).
 - ¹⁷ V. A. Zyuzin, In-plane Hall effect in two-dimensional helical electron systems, *Phys. Rev. B* **102**, 241105(R) (2020).
 - ¹⁸ H. Wang, Y.-X. Huang, H. Liu, X. Feng, J. Zhu, W. Wu, C. Xiao, and S. A. Yang, Orbital origin of the intrinsic planar Hall effect, *Phys. Rev. Lett.* **132**, 056301 (2024).
 - ¹⁹ X.-Q. Yu, Z.-G. Zhu, J.-S. You, T. Low, and G. Su, Topological nonlinear anomalous Nernst effect in strained transition metal dichalcogenides, *Phys. Rev. B* **99**, 201410(R) (2019).
 - ²⁰ C. Zeng, S. Nandy, A. Taraphder, and S. Tewari, Nonlinear Nernst effect in bilayer WTe₂, *Phys. Rev. B* **100**, 245102 (2019).
 - ²¹ Y. Gao and D. Xiao, Orbital magnetic quadrupole moment and nonlinear anomalous thermoelectric transport, *Phys. Rev. B* **98**, 060402(R) (2018).
 - ²² H. Varshney and A. Agarwal, Intrinsic nonlinear Nernst and Seebeck effect, arXiv:2409.111081.
 - ²³ H. Liu, H. Jiang, J. Li, Z. Zhang, X. C. Xie, P. He, J. Zhai, M. Zhang, and J. Shen, Nonlinear Nernst effect in trilayer graphene at zero magnetic field, *Nat. Nanotechnol.* (2025). <https://doi.org/10.1038/s41565-025-01963-8>.
 - ²⁴ C. Zeng, S. Nandy, and S. Tewari, Fundamental relations for anomalous thermoelectric transport coefficients in the nonlinear regime, *Phys. Rev. Res.* **2**, 032066(R) (2020).
 - ²⁵ D.-K. Zhou, Z.-F. Zhang, X.-Q. Yu, Z.-G. Zhu, and G. Su, Fundamental distinction between intrinsic and extrinsic nonlinear thermal Hall effects, *Phys. Rev. B* **105**, L201103 (2022).
 - ²⁶ H. Varshney, K. Das, P. Bhalla, and A. Agarwal, Quantum kinetic theory of nonlinear thermal current, *Phys. Rev. B* **107**, 235419 (2023).
 - ²⁷ H. Varshney, R. Mukherjee, A. Kundu, and A. Agarwal, Intrinsic nonlinear thermal Hall transport of magnons:

- A quantum kinetic theory approach, *Phys. Rev. B* **108**, 165412 (2023).
- ²⁸ Y.-F. Zhang, Z.-F. Zhang, Z.-G. Zhu, and G. Su, Second-order intrinsic Wiedemann-Franz law, *Phys. Rev. B* **111**, 165424(2025).
 - ²⁹ C. Wang, Y. Gao, and D. Xiao, Intrinsic nonlinear Hall effect in antiferromagnetic tetragonal CuMnAs, *Phys. Rev. Lett.* **127**, 277201 (2021).
 - ³⁰ Z.-Y. Zhuang and Z. Yan, Intrinsic nonlinear Hall effect in two-dimensional honeycomb topological antiferromagnets, *Phys. Rev. B* **109**, 174443 (2024).
 - ³¹ N.-Z. Wang, D. Kaplan, Z. Zhang, T. Holder, N. Cao, A. Wang, X. Zhou, F. Zhou, Z. Jiang, C. Zhang, S. Ru, H. Cai, K. Watanabe, T. Taniguchi, B. Yan and W. Gao, Quantum-metric-induced nonlinear transport in a topological antiferromagnet, *Nature* **621**, 487-492 (2023).
 - ³² A. Gao, Y.-F. Liu, J.-X. Qiu, B. Ghosh, T. Trevisan, Y. Onishi, C. Hu, T. Qian, H.-J. Tien, S.-W. Chen, M. Huang, D. Bérubé, H. Li, C. Tzschaschel, T. Dinh, Z. Sun, S.-C. Ho, S.-W. Lien, B. Singh, K. Watanabe, T. Taniguchi, D. C. Bell, H. Lin, T.-R. Chang, C. R. Du, A. Bansil, L. Fu, N. Ni, P. P. Orth, Q. Ma, S.-Y. Xu, Quantum metric nonlinear Hall effect in a topological antiferromagnetic heterostructure, *Science* **381**: 181-186 (2023).
 - ³³ K. Das, S. Lahiri, R. B. Atencia, D. Culcer, and A. Agarwal, Intrinsic nonlinear conductivities induced by the quantum metric, *Phys. Rev. B* **108**, L201405 (2023).
 - ³⁴ K. Das, K. Ghorai, D. Culcer, and A. Agarwal, Nonlinear valley Hall effect, *Phys. Rev. Lett.* **132**, 096302 (2024).
 - ³⁵ Z.-C. Zhou, R.-J. Fang, Z. Zhang, X.-Y. Wang, J.-Y. Rong and X. Li, Nonlinear valley Hall effect in a bilayer transition metal dichalcogenide. arxiv preprint arxiv:2412.19502.
 - ³⁶ H. Watanabe and Y. Yanase, Chiral photocurrent in parity-violating magnet and enhanced response in topological antiferromagnet, *Phys. Rev. X* **11**, 011001 (2021).
 - ³⁷ C. Xiao, H. Liu, J. Zhao, S. A. Yang, and Q. Niu, Thermoelectric generation of orbital magnetization in metals, *Phys. Rev. B* **103**, 045401 (2021).
 - ³⁸ C. Xiao, Y. Ren, and B. Xiong, Adiabatically induced orbital magnetization, *Phys. Rev. B* **103**, 115432 (2021).
 - ³⁹ J. L. Maes, F. Guinea, and María A. H. Vozmediano, Existence and topological stability of Fermi points in multilayered graphene, *Phys. Rev. B* **75**, 155424 (2007).
 - ⁴⁰ S. Latil and L. Henrard, Charge Carriers in Few-Layer Graphene Films, *Phys. Rev. Lett.* **97**, 036803 (2006).
 - ⁴¹ M. Koshino and E. McCann, Parity and valley degeneracy in multilayer graphene, *Phys. Rev. B* **81**, 115315 (2010).
 - ⁴² E. McCann and V. I. Fal'ko, Landau-Level Degeneracy and Quantum Hall Effect in a Graphite Bilayer, *Phys. Rev. Lett.* **96**, 086805 (2006).
 - ⁴³ M. Mucha-Kruczyński, I. L. Aleiner, and V. I. Fal'ko, Strained bilayer graphene: Band structure topology and Landau level spectrum, *Phys. Rev. B* **84**, 041404(R) (2011).
 - ⁴⁴ M. Koshino and T. Ando, Orbital diamagnetism in multilayer graphenes: Systematic study with the effective mass approximation, *Phys. Rev. B* **76**, 085425 (2007).
 - ⁴⁵ E. McCann, M. Koshino, The electronic properties of bilayer graphene, *Rep. Prog. Phys.* **76**, 056503 (2013).
 - ⁴⁶ Y.-L. Wu, G.-H. Zhu, and X.-Q. Yu, Nonlinear anomalous Nernst effect in strained graphene induced by trigonal warping, *Phys. Rev. B* **104**, 195427 (2021).
 - ⁴⁷ R. Battilomo, N. Scopigno, and C. Ortix, Berry Curvature Dipole in Strained Graphene: A Fermi Surface Warping Effect, *Phys. Rev. Lett.* **123**, 196403 (2019).
 - ⁴⁸ J. Xu, W. A. Phelan, and C.-L. Chien, Large Anomalous Nernst Effect in a van der Waals Ferromagnet Fe₃GeTe₂, *Nano Lett.* **19**, 8250 (2019).